Langmuir

Article

pubs.acs.org/Langmuir

Brush/Gold Nanoparticle Hybrids: Effect of Grafting Density on the Particle Uptake and Distribution within Weak Polyelectrolyte Brushes

Stephanie Christau,[†] Tim Möller,[†] Zuleyha Yenice,[†] Jan Genzer,[‡] and Regine von Klitzing*[,†,§]

[†]Stranski Laboratorium für Physikalische Chemie, Technische Universität Berlin, Str. des 17. Juni 124, 10623 Berlin, Germany

[‡]Department of Chemical & Biomolecular Engineering, North Carolina State University, 911 Partners Way, Raleigh, North Carolina 27695-7905, United States

[§]Joint Laboratory for Structural Research (JLSR) of Helmholtz-Zentrum Berlin für Materialien und Energie (HZB), Humboldt-University Berlin, Institut für Physik, Newtonstr. 15, 12489 Berlin, Germany

Supporting Information

ABSTRACT: The effect of the brush grafting density on the loading of 13 nm gold nanoparticles (AuNPs) into stimuli-responsive poly(*N*,*N*-(dimethylamino ethyl) methacrylate) (PDMAEMA) brushes anchored to flat impenetrable substrates is reported. Atom-transfer radical polymerization (ATRP) is used to grow polymer brushes via a "grafting from" approach from a 2-bromo-2-methyl-*N*-(3-(triethoxysilyl) propyl) propanamide (BTPAm)-covered silicon substrate. The grafting density is varied by using mixtures of initiator and a "dummy" molecule that is not able to initiate polymerization. A systematic study is carried out by varying the brush grafting density while keeping all of the other parameters constant. X-ray reflectivity is a suitable tool for investigating the spatial structure of the hybrid, and it is combined with scanning electron microscopy and UV/vis spectroscopy to study the particle loading and interpenetration of the particles within the polymer brush matrix. The particle uptake increases with decreasing grafting density and is highest for an intermediate grafting density because more space between the polymer chains is available. For very low grafting densities of PDMAEMA brushes, the particle uptake decreases because of a lack of the polymer matrix for the attachment of particles. The structure of the surface-grafted polymer chains changes after particle attachment. More water is incorporated into the brush matrix after particle immobilization, which leads to a swelling of the polymer chains in the hybrid material. Water can be removed from the brush by decreasing the relative humidity, which leads to brush shrinking and forces the AuNPs to get closer to each other.

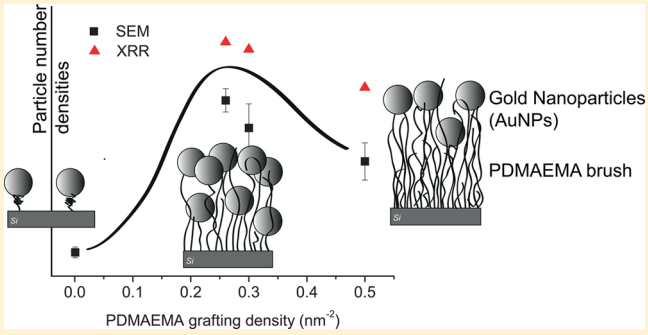

INTRODUCTION

Polymer brushes are defined as macromolecular chains that are end-grafted to a substrate. The structure of a polymer brush depends on the distance between two anchoring polymer chains or, equivalently, on the grafting density of the brushes. At high grafting densities, the polymer chains are forced to stretch out because of segment−segment repulsion, although the entropy opposes stretching ("brush-like" conformation). At low grafting densities, repulsion forces are not as effective, and polymer coils are formed in which conformations are close to those of unperturbed chains ("mushroom" conformation). This phenomenon was first described by Alexander[1] and de Gennes[2] and experimentally proven by Tirell.[3] Polymer brushes respond to external stimuli, such as solvent,[4−7] temperature,[8−10] pH,[11−16] ionic strength,[5,17−19] and voltage.[20] Their responsive nature makes polymer brushes an optimum tool for the development of "smart" surfaces. Potential applications of responsive coatings including polymer brushes can be found in nanotechnology.[21−23] They have been employed as nano-actuators in opening/closing valves by adjusting external conditions such as the temperature[24] and pH.[25] Polymer brush coatings can act as nanoparticle stabilizers/organizers[26] or as antifouling surfaces for biotechnological applications.[27−29] Furthermore, polymer brushes are potential candidates for drug delivery systems[30−34] because of their responsive nature. In the present study, polymer brushes are used as templates for the attachment of gold nanoparticles (AuNPs). Gold particles are known to exhibit surface plasmon resonance (SPR), which arises from the collective oscillation of the conduction electrons in the electromagnetic field of the incident light.[35] This phenomenon is dependent on the size, shape, solvent, core charge, surface ligand, temperature, and proximity of other AuNPs.[36] The particles will induce optical properties within the brush, creating brush/particle hybrids with great potential for

Received: August 27, 2014
Revised: September 28, 2014
Published: October 2, 2014

optical sensor applications. For control of the particle distance, the density of polymers in the matrix plays an important role that, in case of polymer brushes, can be adjusted by varying the brush grafting density.

It has been theoretically predicted that the particle uptake within a polymer brush is greatly influenced by the brush grafting density.[37,38] The grafting density, chain length, and particle size determine how deep the particles will penetrate the polymer matrix. Gage and coworkers studied the adsorption of nanocolloidal SiO_2 particles of ~8 nm diameter into poly(ethylene oxide) (PEO) brushes.[39] The loading of SiO_2 was shown to be strongly affected by the brush grafting density. The highest particle uptake was observed at intermediate grafting densities (of around 0.2 nm^{-2}). A similar grafting density dependence was confirmed by Bhat and coworkers using poly(*N*-isopropylacrylamide) (PNIPAM) brushes.[40] The uptake of gold nanoparticles (AuNPs) of 3.5 nm diameter initially increased with increasing grafting density of the polymer brush and then reached a maximum at an intermediate grafting density (of around 0.38 nm^{-2}) and finally decreased again for very high grafting densities (of around 0.45 nm^{-2}). Bhat and coworkers also studied gold particle uptake in poly(2-(dimethylamino)ethyl methacrylate) (PDMAEMA) brushes.[41] Orthogonal gradients in the molecular weight and grafting density were utilized for the immobilization of 17 nm AuNPs, but contrary to the results obtained for the PNIPAM brushes and the publication by Gage and coworkers, the loading of attached AuNPs increased along the gradient of increasing grafting density. There can be several reasons for the difference, i.e., the gradient brush samples could exhibit a grafting density regime that is lower than the intermediate regime of maximum uptake (no values for the grafting density were given), or there could be a complex interplay among the thickness, grafting density, and large particle size. Because two different polymers, a neutral PNIPAM and a weak polyelectrolyte PDMAEMA, have been studied in the aforementioned publications, the nature of the polymer/particle interactions and the conformation of the polymer in the brush itself could also play important roles. PNIPAM will interact with the citrate coating of the particles via hydrogen bonding whereas the interaction between PDMAEMA and the negatively charged particles will be primarily electrostatic in nature with an additional contribution from hydrogen bonding. The strength of interaction will clearly influence the particle uptake.[42] The particle uptake in PDMAEMA could be different compared to that of neutral polymers because of the strong interaction between particles and polyelectrolyte. The particle uptake will also depend on the brush thickness.[37,43] In fact, the brush thickness should be greater than the size of the particles to allow any penetration. The brush thicknesses in the studies of Bhat and coworkers were in the range of the particle size or even smaller. The role of the brush grafting density on particle interpenetration is addressed in this work, and the dry thickness is adjusted to be at least 2 times larger than the particle size.

Four samples are prepared, having a very high grafting density, two intermediate grafting densities, and a very low grafting density (0.50, 0.30, 0.26, and 0.0008 nm^{-2}). The effect of the polymer grafting density on particle loading is studied, and a model for the structure of PDMAEMA/AuNP hybrids for different grafting densities is elaborated. Ellipsometry, scanning force microscopy, X-ray reflectivity, and scanning electron microscopy are combined to gain a better understanding of the inner structure of the hybrid and the spatial distribution of AuNPs in the PDMAEMA brush matrix. X-ray reflectivity allows us to study the spatial structure of the brush/particle hybrids and reveals greater numbers of particles for both surface-attached and more deeply immobilized AuNPs, for the intermediate grafting densities compared to the very high grafting density. In addition, X-ray reflectivity allows the detection of structural changes in the polymer matrix after the attachment of AuNPs. UV/vis spectroscopy experiments are carried out to monitor the surface plasmon resonance peak of the immobilized particles as a function of the grafting density.

EXPERIMENTAL SECTION

Synthesis. Two steps are needed to synthesize polymer brushes via the grafting from method involving the generation of (1) an initiator-coated self-assembled monolayer (SAM) and (2) surface-initiated polymerization. The polymer brush grafting density can be tuned by adjusting the initiator coverage of the samples. This can be achieved by performing the initiation using mixtures of initiator and a "dummy" molecule that is not able to initiate polymerization.[44−47] Different initiator/dummy ratios were used to obtain different grafting densities.

Chemicals. All chemicals used for the synthesis were received from Aldrich and used without further purification.

Synhesis of PDMAEMA Brushes with Varying Grafting Densities. As a first step, the substrates were etched using piranha solution (H_2SO_4/H_2O_2 1:1 v/v %). As the initiator, 2-bromo-2-methyl-*N*-(3-(triethoxysilyl) propyl) propanamide (BTPAm) was used. Initiator synthesis was performed according to a literature procedure and is described elsewhere.[48] Because of the structural similarity to initiator BTPAm, trimethoxy(propyl)silane (TMS) was used as the dummy molecule. The freshly cleaned substrates were placed into BTPAm/TMS solutions in anhydrous toluene with varying molar ratios of BTPAm/TMS (1:1000, 1:10, 1:1, 1:0) for 24 h at room temperature. After this, the samples were sonicated in toluene for 5 min, rinsed with ethanol, and dried under a stream of nitrogen. Atom-transer radical polymerization (ATRP) of 2-(dimethylamino methacrylate) (DMAEMA) was carried out according to procedures in the literature[49] using a new type of sealed reactor developed by the authors, which was introduced earlier.[43] The original literature recipe was modified by changing the $CuCl/CuCl_2$ ratio to 14:1 in order to slow down the reaction to achieve a better control over the polymerization. The reaction protocol is described elsewhere.[43] Using the reactor allows the polymerization of samples simultaneously in the same polymerization solutions, which ensures that only one parameter of the system (initiator coverage) is being varied.

Synthesis of AuNPs. Spherical citrate-stabilized AuNPs were prepared accoring to a procedure reported by Enüstün and Turkevich.[50] The synthesis procedure is described elsewhere.[51] The diameter of particles was found to be 13.24 ± 0.86 nm as determined by TEM (Supporting Information) using image processing (ImageJ, Wayne Rasband, National Institutes of Health, Bethesda, MD, USA).

PDMAEMA/AuNP Hybrids. AuNPs are adsorbed by the incubation of the PDMAEMA brush samples into the AuNP solution for several hours. To achieve the same conditions (incubation time and temperature, sample tilting) for the different samples, a Teflon vessel was used in which all samples can be incubated simultaneously. After incubation, the samples were removed, sonicated in Milli-Q water for 5 min to remove loosely attached particles, cleaned with ultrapure water (Milli-Q, >19 mΩ cm) twice, and dried with nitrogen.

Instruments. *Ellipsometry.* Ellipsometric measurements were performed with a polarizer-compensator-sample-analyzer (PCSA) ellipsometer (Optrel GbR, Sinzing, Germany) that works at a wavelength of 632.8 nm with an angle of incidence of 70° (near the Brewster angle of the Si/air interface). For data manipulation, Ellipsometry: Simulation and Data Evaluation software (Optrel, v. 3.1) was used. A two-layer-model with air as the front (continuum, n = 1.000), silicon as the backing (continuum, n = 3.885−0.180i), silicon oxide as the first layer (h = 1.5 nm, n = 1.460), and the brush coating as the second layer (n = 1.500) was used to fit the ellipsometric data.

dx.doi.org/10.1021/la503432x | *Langmuir* 2014, 30, 13033−13041

Atomic-Force Microscopy (AFM). Topographic imaging was carried out in air at room temperature with a Cypher AFM (Asylum Research, Santa Barbara, CA, USA) at scan rates of between 1 and 2 Hz. For imaging, Al-coated silicon cantilevers (Olympus, Tokyo, Japan) with a resonance frequency of 320 Hz, a tip radius of 10 nm, a length of 160 μm, and a force constant of 42 N/m were used. Asylum Research Software, a package of IgorPro (Wavemetrics, Inc.), was used for data analysis. The surface roughness was calculated using the formula

$$\sigma_{\mathrm{RMS}} = \sqrt{\left(\frac{1}{N}\sum y_i^2\right)} \tag{1}$$

where σ_{RMS} is the root-mean-square roughness of the considered scan area, N is the number of pixels in this area, and y_i is the z value of a specific pixel. To correct any tilting of the samples, all AFM images were corrected using a line fit. The reported roughness was calculated out of three AFM measurements that were taken at different positions of the wafer.

X-ray Reflectivity (XRR). Measurements were carried out using a Bruker-AXS D8 Discover XRD diffraction system (Bruker AXS GmbH, Karlsruhe, Germany) long-fine focus KFLCu2K tube at $\lambda_{\mathrm{Cu\ K}\alpha}$ = 0.1542 nm. X-ray data were fitted with IgorPro (Wavemetrics, OR) package Motofit.[52] The specular reflectivity is calculated using the Abeles[53] formulation as a function of the perpendicular momentum transfer Q_z,

$$Q_z = \frac{4\pi}{\lambda}\sin\theta$$

The measured specular reflectivity (R) represents the ratio of reflected intensity and incident intensity. A layer model was used to fitting the data with silicon as the backing (SLD = 20.1 × 10^{-6} Å $^{-2}$), air as fronting (SLD = 0 Å^{-2}), and silicon oxide as the first layer (h = 1.5 nm, SLD = 18.9 × 10^{-6} Å^{-2}). For pure PDMAEMA brushes, one additional layer was added. For the polymer/brush particle hybrids, a three-layer model was used to fit the XRR data. Measurements at <8% relative humidity were carried out in a home-built humidity cell. Silica gel was used as a desiccant to control the humidity in the cell.

Scanning Electron Microscopy (SEM). SEM measurements were carried out using a Zeiss DSM 982 GEMINI (Oberkochen, Germany) using acceleration voltages of 10 kV.

Transmission Electron Microscopy (TEM). The samples were prepared using 5 μL of gold particle solution on a TEM copper grid with a carbon support film (200 mesh, Science Services, Munich, Germany) that was pretreated using 10 s of a glow discharge. After a sample was dried, inserting into the sample holder (EM21010, JEOL GmbH, Eching, Germany), and transferring to a JEOL JEM 2100 (JEOL GmbH, Eching, Germany), TEM was carried out at an acceleration voltage of 200 kV. Images were recorded digitally using a bottom-mounted 4k × 4k CMOS camera system (TemCam-F416, TVIPS, Gauting, Germany) and processed with a digital imaging processing system (EM-Menu4.0, TVIPS, Gauting, Germany).

UV/Vis Spectroscopy. UV/vis spectra were recorded using a UV/vis spectrophotometer (PerkinElmer Inc., Waltham, MA, USA) at a temperature of ∼25 °C.

RESULTS

PDMAEMA Brushes. The grafting density σ and distance d between anchoring grafting points can be calculated using

$$\sigma = \frac{\rho_{\mathrm{m}} N_{\mathrm{A}} h_{\mathrm{dry}}}{M_{\mathrm{n}}} \tag{2}$$

$$d \approx \sqrt{\frac{1}{\sigma}} \tag{3}$$

where ρ_{m} is the mass density of DMAEMA (1.318 g/cm^3), N_{A} is Avogadro's number, h_{dry} is the dry thickness of the brushes, and M_{n} is the average molecular weight of the tethered polymer chains.[6,48] Assuming a brush grafting density of σ = 0.50 nm^{-2} for maximum initiator density sample S4 (a typical value for brushes synthesized by the grafting from method[6,40]), we can estimate the molecular weight of the grafted chains from the dry brush thickness using eq 2 ($M_{\mathrm{n}} \approx$ 96 kDa). The grafting densities of S2 and S3 can be estimated using eq 2, assuming that the molecular weight of the grown polymer chains is independent of the initiator density. Note that all of the grafting densities in this work are given under the assumption that S4 = 0.5 nm^{-2}.

Grafting densities and estimated distances between two neighboring polymer chains are listed in Table 1. The dry thickness increases as a function of grafting density. AFM measurements (Figure 1) show that the polymer chains are in the brush-like regime for σ = 0.26, 0.30, and 0.50, denoted as samples S2−S4. The AFM surface roughness is nearly independent of the grafting density (1.8 nm for S2, 1.8 nm for S3, and 2.0 nm for S4).

Table 1. Properties of PDMAEMA Brushes Prepared Using Different Molar Ratios of Initiator/Dummy BTPAm/TMS[a]

sample	initiator/dummy	h_{XRR} (nm)	ρ_e (Å^{-3})	h_{dry} (nm)	σ (nm^{-2})	d (nm)
S1	1:1000				0.0008	36.4
S2	1:10	32	0.33	31 ± 0.4	0.26	2.0
S3	1:1	36	0.34	37 ± 0.6	0.30	1.8
S4	1:0	63	0.37	61 ± 1.3	0.50	1.4

[a]Brush thickness h_{XRR} and electron density ρ_e obtained by X-ray reflectivity and ellispometric thickness h_{dry} measured at <2% RH, from which the grafting density σ and average distance d between two anchored polymer chains was obtained (eq 2). All samples have the same estimated molecular weight of 96 kDa. d and σ for S1 were determined using AFM.

For the sample with the lowest grafting density (S1), it can be assumed that the system has entered a mushroom-like regime (Figure 1). Because of the high heterogeneity accompanied by the low thickness of that sample, ellipsometry cannot be used to determine the thickness. A rough estimation of the grafting density of S1 can be made by analyzing a section graph of the AFM height image (Figure 1e). The distance between two mushrooms is found to be 36 ± 7 nm, which would correspond to a grafting density of ∼0.0008 nm^{-2}.

X-ray Reflectivity (XRR) under Ambient Conditions. XRR measurements were carried out to determine the electron densities of the samples (Figure 2). Data fitting was implemented using one-box models (Gaussian roughness). The fit results are shown in Table 1. The thickness increases with increasing brush grafting density, as does the electron density (inset in Figure 2). It was not possible to fit data for sample S1 (lowest grafting density). This is due to the highly in-plane heterogeneous sample (AFM images, Figure 1) that contributed to a substantial decrease in the specular reflectivity signal (XRR data of S1 shown in the Supporting Information).

PDMAEMA/AuNP Hybrids. *Scanning Electron Microscopy (SEM).* A high particle uptake is observed in the brush-like regime whereas the particle loading in the mushroom regime is very low (Figure 3). The particles are uniformely distributed for all grafting densities of PDMAEMA brushes.

X-ray Reflectivity (XRR) under Ambient Conditions. Reflectivity data and best fits for PDMAEMA/AuNP hybrids with three different grafting densities are shown in Figure 3e, and the results are summarized in Table 2. A three-layer model was used to fit the XRR data. Layer 1 is assigned as the layer

dx.doi.org/10.1021/la503432x | Langmuir 2014, 30, 13033−13041

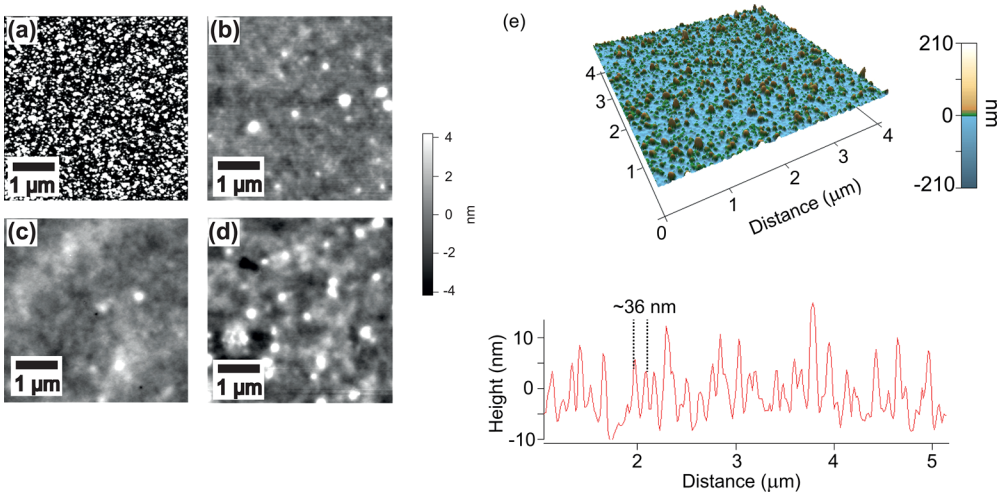

Figure 1. AFM height images of PDMAEMA brushes with different brush grafting densities obtained from BTPAm/TMS molar ratios of (a) 1:1000, (b) 1:10, (c) 1:1, and (d) 1:0 measured under ambient conditions. (e) Three-dimensional AFM height image and AFM section graph of mushroom sample S1, measured under ambient conditions.

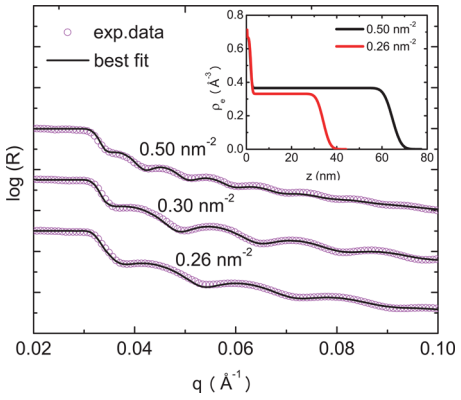

Figure 2. XRR data and best fits for three different grafting densities (top to bottom: 0.50, 0.30, and 0.26 nm^{-2}) measured under ambient conditions. Electron density profiles in the z direction away from the substrate for σ = 0.50 and 0.26 nm^{-2} (inset).

Table 2. XRR Fit Results for PDMAEMA/AuNP Hybrids Measured under Ambient Conditions Using a Three-Layer Fit Model for Three Different Grafting Densities[a]

		XRR layer 1		XRR layer 2		XRR layer 3	
sample	h_{Hyb} (nm)	h_1 (nm)	$\rho_{e,1}$ (Å^{-3})	h_2 (nm)	$\rho_{e,2}$ (Å^{-3})	h_3 (nm)	$\rho_{e,3}$ (Å^{-3})
S2	47.9	38.6	0.69	7.5	2.08	1.7	0.35
S3	50.3	41.2	0.65	7.4	2.00	1.7	0.33
S4	83.3	71.4	0.53	8.4	1.67	3.5	0.13

[a] h is the thickness and ρ_e is the electron density of the respective layer. The total thickness of the hybrid is $h_{Hyb} = h_1 + h_2 + h_3$. χ^2 values of the fits are χ^2 = 0.021 for S4, χ^2 = 0.007 for S3, and χ^2 = 0.011 for S2.

closest to the substrate, layer 2 consists of a particle layer attached to the brush surface, and layer 3 is needed because the particles are protruding out of the brush matrix.[43] Electron density profiles reveal that a large number of particles have been attached to the brush surface in terms of a sharply increasing electron density in that region (inset in Figure 3). In comparing the electron density profiles for σ = 0.5 and 0.26 nm^{-2}, we find that more particles are attached for the intermediate grafting density (value of the electron density is higher). For the highest grafting density, the thickness of layers 2 and 3 together is in the range of the particle size (~13 nm). This reveals that the particles form a monolayer on top of the brushes. For lower grafting densities, the thickness of layer 3 is

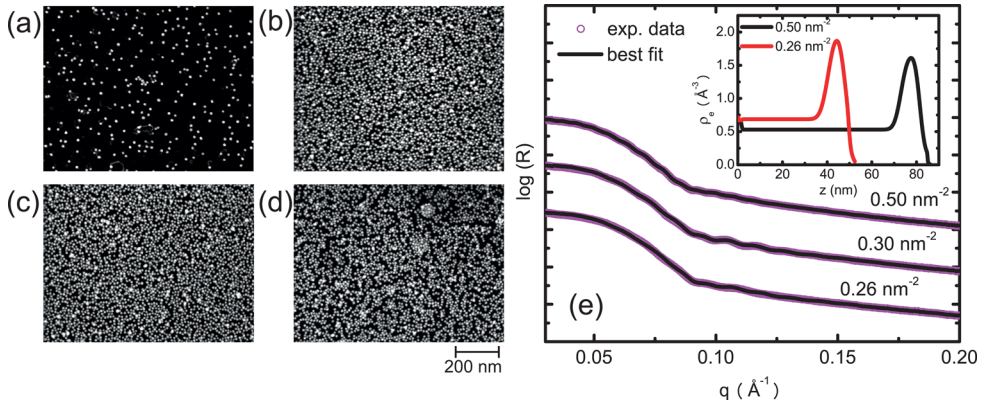

Figure 3. SEM imges of PDMAEMA/AuNP hybrids with brush grafting densities of (a) 0.0008 nm^{-2}, (b) 0.26 nm^{-2}, (c) 0.30 nm^{-2}, and (d) 0.50 nm^{-2}. (e) XRR data and best fits of PDMAEMA/AuNP hybrids with three different grafting densities (top to bottom: 0.50, 0.30, and 0.26 nm^{-2}). Electron density profiles in the z direction away from the substrate for σ = 0.50 and 0.26 nm^{-2} (inset).

dx.doi.org/10.1021/la503432x | Langmuir 2014, 30, 13033−13041

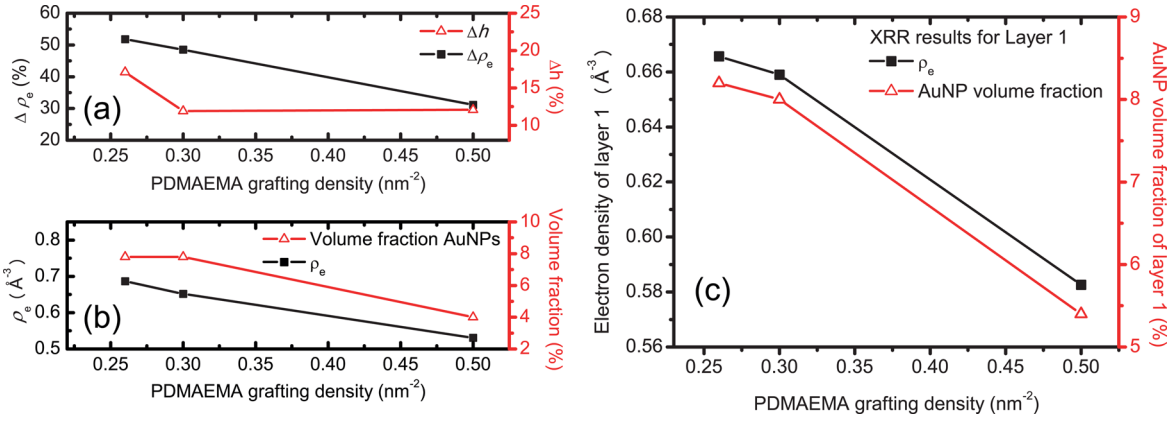

Figure 4. (a) Relative change in electron density $\Delta\rho_e$ of layer 1 and relative change in thickness Δh of layer 1 as a function of the brush grafting density under ambient conditions. (b) Electron density and relative AuNP volume fraction as a function of grafting density under ambient conditions. (c) Electron density and relative AuNP volume fraction of XRR layer 1 as a function of grafting density for RH < 8%.

lower, indicating less particle protrusion. The electron densities of layer 2 are the highest and decrease with increasing grafting density because of the decreased number of attached particles. The electron densities of layer 1 are higher than the respective values of pure PDMAEMA before particle attachment and decrease with increasing grafting density. The thickness of layer 1 after particle attachment is higher than the thickness of pure PDMAEMA before particle adsorption.

To comprehend the reason for the observed swelling of layer 1 after particle attachment, the relative change in electron density $\Delta\rho_e$ of layer 1 and the relative change in thickness Δh of layer 1 compared to pure PDMAEMA were calculated using

$$\Delta\rho_e = \frac{\rho_e(\text{layer 1}) - \rho_e(\text{PDMAEMA})}{\rho_e(\text{layer 1})} \quad (4)$$

$$\Delta h = \frac{h(\text{layer 1}) - h(\text{PDMAEMA})}{h(\text{layer 1})} \quad (5)$$

for each grafting density. A reduction of the relative changes in electron density and thickness is observed with increasing grafting density, but there is no systematic relationship between $\Delta\rho_e$ and Δh (Figure 4a).

If both water and air that might be trapped inside layer 1 are neglected, then the relative volume fractions ϕ of AuNPs can be calculated by exploiting

$$\rho_{e,\text{hybrid}} = \phi_i\rho_{e,i} + (1 - \phi_i)\rho_{e,j} \quad (6)$$

where $\rho_{e,\text{hybrid}}$ is the electron density of the hybrid obtained by fitting the XRR data and ρ_e represents the electron densities of two components i (AuNPs) and j (PDMAEMA). No systematic relationship between the electron density and AuNP volume fraction can be found (Figure 4b).

The fact that there is no simple relationship between Δh and $\Delta\rho_e$ or the AuNP volume fraction and ρ_e indicates a complex interplay among the polymer brush, particles, and water/air inside the brush.

XRR at <8% Relative Humidity. Therefore, X-ray reflectivity experiments were carried out at <8% RH, where the amount of incorporated water is much lower than under ambient conditions. XRR data were fitted using the same layer model as before under ambient conditions. The fit results are shown in Table 3. (For data and best fits, see the Supporting Information.) For all grafting densities of PDMAEMA brushes,

Table 3. XRR Fit Results of PDMAEMA/AuNP Hybrids Measured at Relative Humidities of 4−7% Using a Three-Layer Fit Model for Three Different Grafting Densities[a]

		XRR layer 1		XRR layer 2		XRR layer 3	
sample	h_{Hyb} (nm)	h_1 (nm)	$\rho_{e,1}$ (Å^{-3})	h_2 (nm)	$\rho_{e,2}$ (Å^{-3})	h_3 (nm)	$\rho_{e,3}$ (Å^{-3})
S2	42.4	33.5	0.67	7.8	2.14	1.1	0.33
S3	44.0	34.7	0.66	7.6	2.08	1.8	0.39
S4	71.0	61.1	0.58	8.5	1.81	3.4	0.17

[a] h is the thickness and ρ_e is the electron density of the respective layer. The total thickness of the hybrid is $h_{Hyb} = h_1 + h_2 + h_3$. χ^2 values of the fits are $\chi^2 = 0.022$ for S4, $\chi^2 = 0.011$ for S3, and $\chi^2 = 0.003$ for S2.

the thickness of layer 1 decreases after decreasing the humidity to <8%. The electron densities of layer 1 show a PDMAEMA grafting density dependence: ρ_e of S4 increases by ∼9% whereas ρ_e for S3 is nearly unchanged (∼1% increased). The electron density of S2 decreases by ∼3%. The electron densities of layer 2 increase for all grafting densities (8% for S4 and 4% for S3 and S2). The thicknesses and electron densities of layer 3 do not exhibit any systematic variation. Different from the measurements under ambient conditions, a systematic relationship between the electron densities and AuNP volume fractions of layer 1 can be found (Figure 4c).

Particle Number Densities. Next, SEM and XRR particle number densities will be determined and compared.

The SEM particle number density (particles/μm^2) can be obtained from SEM top-view images (Figure 3) by image processing (ImageJ, Wayne Rasband, National Institute of Health, Bethesda, Maryland, USA). XRR particle numbers were calculated using a box model[43] where

$$\text{number of particles} = \frac{V_{box}}{V_{AuNP}} \quad (7)$$

with $V_{AuNP} = {}^4/_3\pi r^3$ assigned as the volume of a single AuNP with radius r = 6.5 nm. An imaginary box with volume V_{box} and a dimension of 1 μm length/width and 0.013 μm (= particle diameter) is designed (Figure 5a (inset)). The box covers a 1 μm × 1 μm area of the AuNP monolayer. When eq 7 is used, the maximum number of particles within the designed box can be calculated to yield 11 300 particles. This corresponds to a particle volume fraction of 100%. XRR volume fractions can be calculated using eq 6. When these values are used, it is possible

dx.doi.org/10.1021/la503432x | Langmuir 2014, 30, 13033−13041

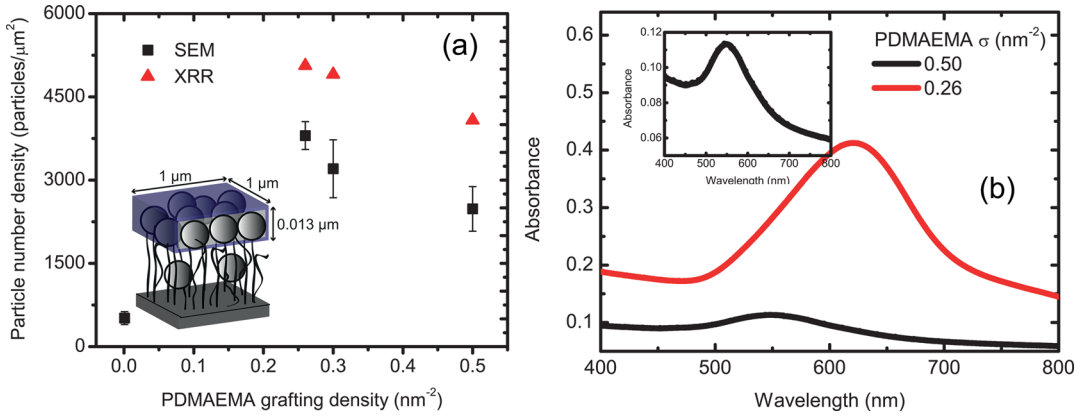

Figure 5. (a) Particle number densities derived from SEM images or XRR using the box model (inset) as a function of the grafting density.(b) UV/vis spectra recorded under ambient conditions for samples obtained for initiator/dummy ratios of 1:0 and 1:10 or σ = 0.5 and 0.26 nm^{-2}, respectively. Magnified representation of the plasmon band for σ = 0.5 nm^{-2} (inset).

to calculate the respective number densities of particles attached within the box. Because the box height is equal to the particle size and the particles form a monolayer on top of the brushes, these values correspond to the particle number densities in terms of particles/μm^2. Number densities calculated from XRR volume fractions using the box model are assigned as XRR particle number densities.

In the brush-like regime, the particle number density decreases with increasing grafting density (Figure 5a). SEM and XRR number densities show the same qualitative behavior although the XRR values are higher. The difference can be explained by considering the roughness of the brush, which compounds SEM image processing. Several particles or small particle aggregates might be counted as one particle, leading to a lower value of the SEM particle number density compared to the XRR particle number density.

UV/Vis Spectroscopy. Brushes with two different grafting densities for initiator/dummy ratios of 1:0 and 1:10 were polymerized on glass substrates for ∼30 min. PDMAEMA/AuNP hybrids were examined under ambient conditions to monitor the surface plasmon resonance peak of the immobilized AuNPs. The UV/vis spectra confirm the results obtained for SEM and XRR. For the medium grafting density of 0.26 nm^{-2}, a higher particle loading is observed than for σ = 0.5 nm^{-2}. The intensity of the plasmon peak increases for decreasing grafting density (Figure 5b). In addition, the peak is broader and shifted to higher wavelengths, a typical indication for high particle crowding that leads to plasmon coupling.[54]

DISCUSSION

Samples featuring different PDMAEMA grafting densities were synthesized using different ratios of inititator BTPAm and dummy molecule TMS. Because TMS acts only as a space-filler and does not promote polymerization, the grafting density can be reduced by decreasing the ratio of initiator/dummy. Negatively charged, citrate-coated gold particles were attached to the PDMAEMA brushes by the incubation of the samples in the particle solution several hours. At the pH of the gold solution (∼5.5−6), PDMAEMA (pK_a 7.5) is mostly protonated.[55,56] Strong ionic attraction with negatively charged AuNPs is expected. A large number of attached particles are confirmed by SEM measurements in the brush-like regime. The particle number density for S2−S4 decreases with increasing grafting density of PDMAEMA. Only a very small number of particles have been attached to sample S1, where PDMAEMA exhibits the mushroom conformation. Here, the lack of a polymer matrix is the reason for the small number of particles.

X-ray reflectivity data for the brush-like samples show that a monolayer of particles is formed on top of the PDMAEMA brushes. A three-layer model was used to fit the XRR data, where layer 1 is assigned as the layer closest to the substrate, followed by surface layer 2 consisting of AuNPs and polymer. Layer 3 arises because the particles are protruding out of the PDMAEMA brush matrix. A smaller thickness for layer 3 was found for S3 and S2. Because of the reduced grafting density, the AuNPs can be embedded more easily. The electron densities for layer 2 increase for a decreasing grafting density, confirming the increasing number densities of AuNPs. Recently, our group investigated the effect of brush thickness on particle uptake.[43] The particle number density was found to increase with increasing brush thickness because of an increased surface roughness (more binding sites become available). In this work, roughness cannot be the reason for increasing particle uptake because the roughness does not change significantly with the grafting density. The electron densities of layer 2 at low humidities are slightly higher than the electron densities under ambient conditions. While the water is removed, the brush shrinks, therefore dragging the attached particles down and forcing them to come closer to each other.

Interestingly, the thicknesses of layer 1 are greater than the initial PDMAEMA brush thicknesses before particle attachment, and the electron densities of layer 1 decrease with increasing grafting density. Both observations could be explained by a greater number of particles inside layer 1 for a lower grafting density. If this were true, then there should be a systematic relationship between the electron density of layer 1 and the AuNP volume fraction. This is not the case, which indicates additional water or air inside layer 1 after AuNP immobilization.

In contrast, after the water was removed, a systematic relationship between the electron density of layer 1 and the AuNP volume fraction was observed (Figure 4c). XRR measurements carried out at 4−7% RH show a reduced thickness of layer 1 for all grafting densities compared to XRR under ambient conditions, which is in the same range for all grafting densities (Δh = 14% for S4, 16% for S3, and 13% for S2).

dx.doi.org/10.1021/la503432x | *Langmuir* 2014, 30, 13033−13041

The electron densities of layer 1 change after reducing the humidity and show grafting-density-dependent yet non-systematic behavior. The electron densities of layer 1 increase by 9% for S4 and by 1% for S3 and decrease by 3% for S2. This nonsystematic behavior can be explained by taking into account the electron density of incorporated water (0.34 $Å^{-3}$, Motofit Database). The electron density of water compared to that of pure PDMAEMA is (1) lower than the electron density of S4 (0.37 Å), (2) the same for S3 (0.34 Å), and (3) slightly higher for S2 (0.33 Å). Subsequently, the electron density of pure PDMAEMA brushes after removing the water increases by 8% for S4, remains unchanged for S3, and slightly decreases by 3% for S2. This is illustrated in Figure 6 in terms of the ratio between the electron density of PDMAEMA and water, ρ_e (PDMAEMA)/ρ_e (H_2O).

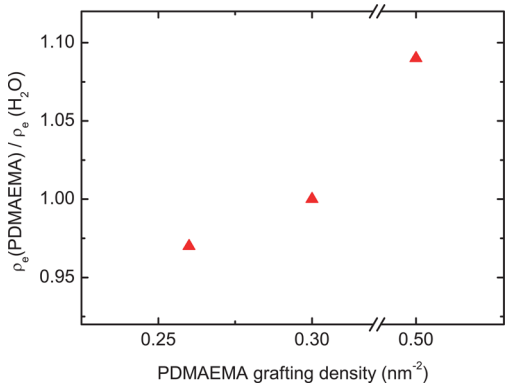

Figure 6. Ratio of the electron density of PDMAEMA brushes ρ_e (PDMAEMA) and the electron density of water ρ_e (H_2O) as a function of the PDMAEMA grafting density.

There is good agreement among the experimental values of PDMAEMA/AuNP layer 1 (9, 1, and 3%), which leads to the conclusion that the swelling of layer 1 after particle attachment arises from incorporated water under ambient conditions. Slight variations can be explained by the fact that (1) even at humdities of <8% a small amount of water will be trapped inside the brushes and (2) the electron densities of pure PDMAEMA were obtained by XRR measurements under ambient conditions.

A possible explanation for left-over water is the formation of cavities inside the polymer matrix, which can arise from the incorporation of the particles. After removing the sample from the AuNP solution, these cavities will still be filled with water and will lead to an increase in thickness.

Considering the results obtained by SEM, XRR, and ellipsometry, a model for the structure of PDMAEMA/AuNP hybrids can be derived (Figure 7). For all PDMAEMA grafting densities in the brushlike regime, a monolayer of AuNPs is formed on the brush surface. For very low grafting densities (mushroom-like regime), the particle uptake is low because of the lack of polymer binding sites (Figure 7a). For intermediate grafting densities, a high particle uptake is observed (Figure 7b). AuNPs are attached to the brush surface and penetrate the brush more deeply than for very high grafting densities (Figure 7c). For a very high grafting density (0.5 nm^{-2}), only a small number of particles penetrate the PDMAEMA brush because of the high osmotic pressure. AuNPs attached to the brush surface protrude out of the brush. UV/vis measurements confirm the results obtained by XRR and SEM in terms of an increasing

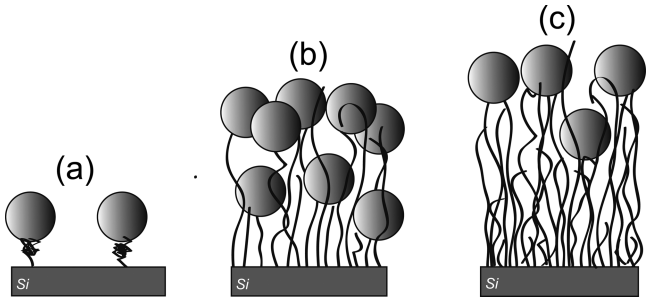

Figure 7. Model for the structure of PDMAEMA/AuNP hybrids for (a) a very low grafting density, (b) intermediate grafting densities, and (c) high grafting densities.

plasmon intensity for the medium grafting density compared to a very high grafting density.

In the present study, the highest particle uptake of 13 nm AuNPs in PDMAEMA brushes was observed for grafting densities of around 0.26 nm^{-2}. As mentioned earlier, previous work involving PEO brushes with immobilized 8 nm SiO_2 NPs[39] reported a maximum particle uptake at grafting densities of around 0.20 nm^{-2}. For small 3.5 nm AuNPs in PNIPAM brushes,[40] the maximum loading was found at grafting densities of around 0.38 nm^{-2}. This shows that the grafting density dependency of the uptake and penetration of NPs in brush matrices is highly dependent on the nature of the polymer (neutral polymer vs weak/strong polyelectrolyte) and particles as well as the particle size and the strength of the polymer–particle interaction. In the case of PDMAEMA, a strong electrostatic attraction between the positively charged polymer and the negatively charged particles leads to a high particle uptake; opposed to that, electrostatic repulsion between charged AuNPs could lead to a blocking effect where further particle attachment is hindered by already-attached particles. The former promotes particle uptake whereas the latter is a limiting factor.

■ CONCLUSIONS

The effect of the brush grafting density on the uptake of 13 nm AuNPs into PDMAEMA brushes was investigated. For very high grafting densities of PDMAEMA, AuNP attachment and penetration is limited by the high osmotic pressure in the brush and steric hindrance. The particle uptake increases for decreasing grafting densities. A high particle uptake and better particle penetration were found for medium grafting densities of PDMAEMA grafts. The particles form a monolayer attached to the brush surface for all samples in the brush-like regime. For very low PDMAEMA grafting densities (mushroom regime), the AuNP uptake is very low because of the lack of a polymer matrix. The structure of the surface-anchored PDMAEMA chains changes because of particle attachment; the thickness is increased by incorporated water that arises from cavity formation after AuNP immobilization. Water could be removed by decreasing the relative humidity, which leads to brush shrinking and forces the particles to get closer.

The topic of PDMAEMA/AuNP hybrid brushes addresses the general question of the impact of electrostatic attraction and repulsion forces in hybrid systems. Further studies will be carried out elaborating the effect of charge (using polyelectrolytes vs neutral polymers and charged vs non-charged particles) on particle loading and penetration.

dx.doi.org/10.1021/la503432x | Langmuir 2014, 30, 13033−13041

■ ASSOCIATED CONTENT

Supporting Information

TEM images of AuNPs, XRR data of sample S1 before and after particle attachment, and XRR data for low RH. This material is available free of charge via the Internet at http://pubs.acs.org.

■ AUTHOR INFORMATION

Corresponding Author

*E-mail: klitzing@mailbox.tu-berlin.de.

Notes

The authors declare no competing financial interest.

■ ACKNOWLEDGMENTS

We thank Christoph Fahrenson (Zentraleinrichtung für Elektronenmikroskopie (ZELMI, TU Berlin)) for SEM measurements and Sarah T. Turner for TEM measurements. TEM experiments were carried out at the electron microscope of Joint Laboratory for Structural Research (JLSR) of Helmholtz-Zentrum Berlin für Materialien und Energie (HZB), Humboldt-Universität zu Berlin (HU) and Technische Universität Berlin (TU). Finanical support was granted by the German Science Foundation (DFG) via International Research Training Group (IRTG) 1524 at the Technische Universität Berlin.

■ REFERENCES

(1) Alexander, S. Polymer adsorption on small spheres. A scaling approach. *J. Phys. (Paris)* **1977**, *38*, 977.

(2) de Gennes, P. Conformations of Polymers Attached to an Interface. *Macromolecules* **1980**, *13*, 1069−1075.

(3) Hadziioannou, G.; Patel, S.; Granick, S.; Tirrell, M. Forces between surfaces of block copolymers adsorbed on mica. *J. Am. Chem. Soc.* **1986**, *108*, 2869−2876.

(4) Ross, R. S.; Pincus, P. The polyelectrolyte brush: poor solvent. *Macromolecules* **1992**, *25*, 2177−2183.

(5) Biesalski, M.; Johannsmann, D.; Ruehe, J. Synthesis and swelling behavior of a weak polyacid brush. *J. Chem. Phys.* **2002**, *117*, 4988.

(6) Sanjuan, S.; Perrin, P.; Pantoustier, N.; Tran, Y. Synthesis and swelling behavior of pH-responsive polybase brushes. *Langmuir* **2007**, *23*, 5769−78.

(7) Oren, R.; Liang, Z.; Barnard, J. S.; Warren, S. C.; Wiesner, U.; Huck, W. T. S. Organization of nanoparticles in polymer brushes. *J. Am. Chem. Soc.* **2009**, *131*, 1670−1.

(8) Balamurugan, S.; Mendez, S.; Balamurugan, S. S.; O'Brien, M. J., II; Lopez, G. P. Thermal Response of Poly (N-isopropylacrylamide) Brushes Probed by Surface Plasmon Resonance. *Langmuir* **2003**, *19*, 2545−2549.

(9) Yim, H.; Kent, M. S.; Mendez, S.; Balamurugan, S. S.; Balamurugan, S.; Lopez, G. P.; Satija, S. Temperature-Dependent Conformational Change of PNIPAM Grafted Chains at High Surface Density in Water. *Macromolecules* **2004**, *37*, 1994−1997.

(10) Liu, G.; Zhang, G. Collapse and swelling of thermally sensitive poly(N-isopropylacrylamide) brushes monitored with a quartz crystal microbalance. *J. Phys. Chem. B* **2005**, *109*, 743−7.

(11) An, S. W.; Thirtle, P. N.; Thomas, R. K.; Baines, F. L.; Billingham, N. C.; Armes, S. P.; Penfold, J. Structure of a Diblock Copolymer Adsorbed at the Hydrophobic Solid/Aqueous Interface: Effects of Charge Density on a Weak Polyelectrolyte Brush. *Macromolecules* **1999**, *32*, 2731−2738.

(12) Houbenov, N.; Minko, S.; Stamm, M. Mixed Polyelectrolyte Brush from Oppositely Charged Polymers for Switching of Surface Charge and Composition in Aqueous Environment. *Macromolecules* **2003**, *36*, 5897−5901.

(13) Geoghegan, M.; Ruiz-Pérez, L.; Dang, C. C.; Parnell, A. J.; Martin, S. J.; Howse, J. R.; Jones, R. a. L.; Golestanian, R.; Topham, P. D.; Crook, C. J.; Ryan, A. J.; Sivia, D. S.; Webster, J. R. P.; Menelle, A. The pH-induced swelling and collapse of a polybase brush synthesized by atom transfer radical polymerization. *Soft Matter* **2006**, *2*, 1076.

(14) Plamper, F. A.; Schmalz, A.; Ballauff, M.; Mu, A. H. E. Tuning the Thermoresponsiveness of Weak Polyelectrolytes by pH and Light: Lower and Upper Critical-Solution Temperature of Poly(N,N -dimethylaminoethyl methacrylate). *J. Am. Chem. Soc.* **2007**, *129*, 14538−14539.

(15) Hinrichs, K.; Aulich, D.; Ionov, L.; Esser, N.; Eichhorn, K.-J.; Motornov, M.; Stamm, M.; Minko, S. Chemical and structural changes in a pH-responsive mixed polyelectrolyte brush studied by infrared ellipsometry. *Langmuir* **2009**, *25*, 10987−91.

(16) Jia, H.; Wildes, A.; Titmuss, S. Structure of pH-Responsive Polymer Brushes Grown at the GoldWater Interface: Dependence on Grafting Density and Temperature. *Macromolecules* **2012**, *45*, 305−312.

(17) Currie, E. P. K.; Sieval, a. B.; Fleer, G. J.; Cohen Stuart, M. A. Polyacrylic Acid Brushes:, Surface Pressure and Salt-Induced Swelling. *Langmuir* **2000**, *16*, 8324−8333.

(18) Mouri, E.; Kaewsaiha, P.; Matsumoto, K.; Matsuoka, H.; Torikai, N. Effect of salt concentration on the nanostructure of weak polyacid brush in the amphiphilic polymer monolayer at the air/water interface. *Langmuir* **2004**, *20*, 10604−11.

(19) Zhang, H.; Ruehe, J. Swelling of Poly(methacrylic acid) Brushes: Influence of Monovalent Salts in the Environment. *Macromolecules* **2005**, *38*, 4855−4860.

(20) Weir, M. P.; Heriot, S. Y.; Martin, S. J.; Parnell, A. J.; Holt, S. a.; Webster, J. R. P.; Jones, R. a. L. Voltage-induced swelling and deswelling of weak polybase brushes. *Langmuir* **2011**, *27*, 11000−7.

(21) Gupta, S.; Agrawal, M.; Uhlmann, P.; Simon, F.; Oertel, U.; Stamm, M. Gold Nanoparticles Immobilized on Stimuli Responsive Polymer Brushes as Nanosensors. *Macromolecules* **2008**, *41*, 8152−8158.

(22) Mitsuishi, M.; Koishikawa, Y.; Tanaka, H.; Sato, E.; Mikayama, T.; Matsui, J.; Miyashita, T. Nanoscale actuation of thermoreversible polymer brushes coupled with localized surface plasmon resonance of gold nanoparticles. *Langmuir* **2007**, *23*, 7472−4.

(23) Tokareva, I.; Minko, S.; Fendler, J. H.; Hutter, E. Nanosensors based on responsive polymer brushes and gold nanoparticle enhanced transmission surface plasmon resonance spectroscopy. *J. Am. Chem. Soc.* **2004**, *126*, 15950−1.

(24) Park, Y. S.; Ito, Y.; Imanishi, Y. Permeation Control through Porous Membranes Immobilized with Thermosensitive Polymer. *Langmuir* **1998**, *14*, 910−914.

(25) Zhang, H.; Ito, Y. pH Control of Transport through a Porous Membrane Self-Assembled with a Poly (acrylic acid) Loop Brush. *Langmuir* **2001**, *17*, 8766−8770.

(26) Snaith, H. J.; Whiting, G. L.; Sun, B.; Greenham, N. C.; Huck, W. T. S.; Friend, R. H. Self-organization of nanocrystals in polymer brushes. Application in heterojunction photovoltaic diodes. *Nano Lett.* **2005**, *5*, 1653−7.

(27) Ista, L. K.; Lopez, G. P. Lower critical solubility temperature materials as biofouling release agents. *J. Ind. Microbiol. Biotechnol.* **1998**, *20*, 121−125.

(28) Senaratne, W.; Andruzzi, L.; Ober, C. K. Self-assembled monolayers and polymer brushes in biotechnology: current applications and future perspectives. *Biomacromolecules* **2005**, *6*, 2427−48.

(29) Fristrup, C. J.; Jankova, K.; Hvilsted, S. r. Surface-initiated atom transfer radical polymerization technique to develop biofunctional coatings. *Soft Matter* **2009**, *5*, 4623.

(30) Diamanti, S.; Arifuzzaman, S.; Genzer, J.; Vaia, R. A. Capture and Release. *ACS Nano* **2009**, *3*, 807−818.

(31) Motornov, M.; Tam, T. K.; Pita, M.; Tokarev, I.; Katz, E.; Minko, S. Switchable selectivity for gating ion transport with mixed polyelectrolyte brushes: approaching 'smart' drug delivery systems. *Nanotechnology* **2009**, *20*, 434006.

(32) Bajpai, A. K.; Shukla, S. K.; Bhanu, S.; Kankane, S. Responsive polymers in controlled drug delivery. *Prog. Polym. Sci.* **2008**, *33*, 1088−1118.

(33) Kost, J.; Langer, R. Responsive polymeric delivery systems. *Adv. Drug Delivery Rev.* **2001**, *46*, 125−48.
(34) Schmaljohann, D. Thermo- and pH-responsive polymers in drug delivery. *Adv. Drug Delivery Rev.* **2006**, *58*, 1655−70.
(35) Yeh, Y.-C.; Creran, B.; Rotello, V. M. Gold nanoparticles: preparation, properties, and applications in bionanotechnology. *Nanoscale* **2012**, *4*, 1871−80.
(36) Hu, M.; Chen, J.; Li, Z.-Y.; Au, L.; Hartland, G. V.; Li, X.; Marquez, M.; Xia, Y. Gold nanostructures: engineering their plasmonic properties for biomedical applications. *Chem. Soc. Rev.* **2006**, *35*, 1084−94.
(37) Kim, J.; O'Shaughnessy, B. Morphology Selection of Nanoparticle Dispersions by Polymer Media. *Phys. Rev. Lett.* **2002**, *89*, 238301.
(38) Kim, J. U.; O'Shaughnessy, B. Nanoinclusions in Dry Polymer Brushes. *Macromolecules* **2006**, *39*, 413−425.
(39) Cage, R. A.; Currie, E. P. K.; Cohen Stuart, M. A. Adsorption of Nanocolloidal SiO_2 Particles on PEO Brushes. *Macromolecules* **2001**, *34*, 5078−5080.
(40) Bhat, R. R.; Genzer, J. Combinatorial study of nanoparticle dispersion in surface-grafted macromolecular gradients. *Appl. Surf. Sci.* **2006**, *252*, 2549−2554.
(41) Bhat, R. R.; Tomlinson, M. R.; Genzer, J. Assembly of Nanoparticles using Surface-Grafted Orthogonal Polymer Gradients. *Macromol. Rapid Commun.* **2004**, *25*, 270−274.
(42) Steels, B. M.; Koska, J.; Haynes, C. A. Analysis of brush-particle interactions using self-consistent-field theory. *J. Chromatogr. B: Biomed. Sci. Appl.* **2000**, *743*, 41−56.
(43) Christau, S.; Thurandt, S.; Yenice, Z.; von Klitzing, R. Stimuli-Responsive Polyelectrolyte Brushes as a Matrix for the Attachment of Gold Nanoparticles: The Effect of Brush Thickness on Particle Distribution. *Polymers* **2014**, *6*, 1877−1896.
(44) Plunkett, K. N.; Zhu, X.; Moore, J. S.; Leckband, D. E. PNIPAM chain collapse depends on the molecular weight and grafting density. *Langmuir* **2006**, *22*, 4259−66.
(45) Kusumo, A.; Bombalski, L.; Lin, Q.; Matyjaszewski, K.; Schneider, J. W.; Tilton, R. D. High capacity, charge-selective protein uptake by polyelectrolyte brushes. *Langmuir* **2007**, *23*, 4448−54.
(46) Takahashi, H.; Nakayama, M.; Yamato, M.; Okano, T. Controlled chain length and graft density of thermoresponsive polymer brushes for optimizing cell sheet harvest. *Biomacromolecules* **2010**, *11*, 1991−9.
(47) Nagase, K.; Kobayashi, J.; Kikuchi, A.; Akiyama, Y.; Kanazawa, H.; Annaka, M.; Okano, T. Preparation of thermoresponsive anionic copolymer brush surfaces for separating basic biomolecules. *Biomacromolecules* **2010**, *11*, 215−23.
(48) Laurent, P.; Souharce, G.; Duchet-Rumeau, J.; Portinha, D.; Charlot, A. 'Pancake' vs. brush-like regime of quaternizable polymer grafts: an efficient tool for nano-templating polyelectrolyte self-assembly. *Soft Matter* **2012**, *8*, 715.
(49) Bain, E. D.; Dawes, K.; Özçam, A. E.; Hu, X.; Gorman, C. B.; Šrogl, J.; Genzer, J. Surface-Initiated Polymerization by Means of Novel, Stable, Non-Ester-Based Radical Initiator. *Macromolecules* **2012**, *45*, 3802−3815.
(50) Enustun, B. V.; Turkevich, J. Coagulation of colloidal gold. *J. Am. Chem. Soc.* **1963**, *85*, 3317−3328.
(51) Karg, M.; Schelero, N.; Oppel, C.; Gradzielski, M.; Hellweg, T.; von Klitzing, R. Versatile phase transfer of gold nanoparticles from aqueous media to different organic media. *Chemistry* **2011**, *17*, 4648−54.
(52) Nelson, A. Co-refinement of multiple-contrast neutron/X-ray reflectivity data using MOTOFIT. *J. Appl. Crystallogr.* **2006**, *39*, 273−276.
(53) Heavens, O. S. Optical properties of thin films. *Rep. Prog. Phys.* **1960**, *23*, 1−65.
(54) Bhat, R. R.; Genzer, J.; Chaney, B. N.; Sugg, H. W.; Liebmann-Vinson, A. Controlling the assembly of nanoparticles using surface grafted molecular and macromolecular gradients. *Nanotechnology* **2003**, *14*, 1145−1152.
(55) Cherng, J. Y.; Talsma, H.; Verrijk, R.; Crommelin, D. J.; Hennink, W. E. The effect of formulation parameters on the size of poly-((2-dimethylamino)ethyl methacrylate)-plasmid complexes. *Eur. J. Pharm. Biopharm.* **1999**, *47*, 215−24.
(56) Bhat, R. R.; Tomlinson, M. R.; Wu, T.; Genzer, J. Surface-Grafted Polymer Gradients: Formation, Characterization, and Applications. *Adv. Polym. Sci.* **2006**, *198*, 51−124.